Statistical analysis of fading power vectors for real-time atmospheric channel emulation

Yousef K. Chahine[1,*], Evan J. Katz[1], Brian E. Vyhnalek[1], and Sarah A. Tedder[1]

[1]NASA Glenn Research Center, Cleveland, Ohio, 44135

ABSTRACT

The design and testing of a free-space optical communication system requires assessment of the impact of random fluctuations in received power from a laser beam transmitted over an atmospheric channel. A number of methods for generating fading power vectors for in-lab emulation of an atmospheric channel have previously been reported. These techniques include spectral shaping and filtering of a signal from a normally distributed pseudo-random number generator, full wave optics simulations with random phase screens, and pre-recorded measurements from experimental free-space links. In this work, a statistical analysis of atmospheric fading is presented with the goal of producing a practical engineering model for the fading channel suitable for generating synthetic fade vectors in real-time for long-duration receiver testing with channel interleaving. Specifically, a parametric model is developed for turbulence-induced fade on space-to-ground links with large-aperture receivers, including aperture-averaging and the effects of aperture size on the instantaneous coupling efficiency for mode-limited receivers. In particular, we analyze the probability density function and temporal power spectrum for fluctuations of the coupling efficiency for few-mode fibers in a range of turbulence conditions.

Keywords: free-space optical communication, atmospheric turbulence, optical fibers

1. INTRODUCTION

One of the primary challenges inherent in free-space optical communication is random fading in the received power signal over a free-space channel. Two significant sources of such fades are beam pointing error and scintillation due to propagation through turbulence in Earth's atmosphere. The nature of these fading signals has been well-documented experimentally and sophisticated analytical models have been developed to understand link performance in a wide range of scenarios.[1–5] On the other hand, for the purposes of controlled system testing it is desirable to have a minimal engineering model for the fading channel so that synthetic power vectors of arbitrary length can be fully characterized and reproduced. For example, NASA Glenn Research Center (GRC) is developing an optical ground receiver for photon-starved applications implementing the Consultative Committee for Space Data Systems (CCSDS) High Photon Efficiency (HPE) standard (the receiver system includes a fiber interconnect, photon-counting detectors, and real-time field programmable gate array based receiver). To test the receiver, including the implementation of fade mitigation techniques based on channel interleaving, it is necessary to operate under realistic conditions including emulation of the fading channel. This can be done in-lab by using a relatively fast modulator to attenuate the optical signal from the test transmitter.[6–8] To obtain the integration times required to characterize codeword error rate (CWER) performance, it is desirable to be able to synthesize fade vectors to modulate the signal continuously in real time for CWER tests that may run for many hours.

In this paper, we develop simplified engineering models for the received power over a fading channel as a random process which can be completely characterized and synthesized in real-time. Although recorded

*yousef.k.chahine@nasa.gov

measurements are typically a gold-standard for testing a receiver in realistic conditions,[6] in many cases a suitable set of data sufficient for long-duration tests in a range of link scenarios is unavailable. A useful approach in this case is to employ wave optics simulations to develop fade vectors for a wider range of conditions;[7] however, that approach is not ideal for controlled long-duration testing as finite-length fade vectors must be generated in advance and the underlying structure of the fading signal is obfuscated by the complexity of the simulations. Conversely, a standard model based on a minimal set of parameters allows for direct comparisons between different receiver implementations without concern over differences in the underlying empirical data or detailed assumptions in the model.

Our approach is motivated by the power vector generation tool presented by Giggenbach *et al.*[9] A simplified channel model is employed where each source of fade is parameterized by the variance of the underlying process, together with a cutoff frequency and low-pass filter slope determining the temporal statistics.[10] However, in that work the parameters were chosen based on a fit to available data from a prior satellite optical downlink.[11] In this paper, we develop a parametric model for a space-to-ground fading channel including a range of link conditions, aperture sizes, and sources of fade for which experimental data may be limited or unavailable. For example, the receiver under development at GRC uses a few-mode fiber interconnect to deliver light to photon-counting detectors. This introduces additional turbulence-induced fluctuations from the instantaneous few-mode fiber coupling efficiency which dominates aperture-averaged scintillation for large-aperture receivers. A statistical analysis of these power fluctuations for receivers coupling to few-mode fibers (given in Section 4) allows these fluctuations in received power to be included in the model of the fading channel used to generate fade vectors. This can greatly simplify the testbed by enabling testing without requiring real-time emulation of the distorted optical wavefront arriving at the pupil plane of the telescope. A model for pointing-induced fluctuations—which also represent a dominant source of fade for large-aperture receivers—is not treated in this work; however, suitable models can be found in the literature.[9,12,13]

In Section 2, we describe the general requirements of the channel model. In Section 3, we employ an engineering approximation for the temporal power spectrum of aperture-averaged scintillation developed by Yura[14] to produce a general parametric model determined by aperture radius and effective Fresnel frequency for slant-path atmospheric channels. In Section 4, we analyze turbulence-induced fluctuations of the instantaneous coupling efficiency for receivers coupling to few-mode fibers. To address the additional complexity inherent in statistically modeling the coupling to few-mode fiber relative to single-mode fiber,[15–17] we combine a theoretical framework for few-mode fiber coupling[18,19] with Monte Carlo simulations using Kolmogorov phase screens[20] to obtain a model for the probability density function (pdf) and temporal power spectrum of these fluctuations.

2. FADING CHANNEL MODELS BASED ON GAUSSIAN PROCESSES

As discussed above, the goal of this work is to develop simplified parametric models for the received power over a fading channel as a random process $X(t)$ which can be completely characterized and synthesized in real-time. A complete description of a random process $X(t)$ generally requires specification of the n-th order pdf for all n,[21] or of the algorithm used to generate the sample vectors. In practice, such complete knowledge is often not available and specification is restricted to some description of the first and second order pdf. For ergodic processes, these are determined by the time-independent first-order pdf $p_X(x)$ and power spectral density (psd) $\Phi_X(\omega)$.

Although complete description of the higher order pdfs is rarely necessary, it is worth noting that for stationary Gaussian processes, the pdf and psd determine all of the higher order pdfs, and so completely specify the process. Additionally, for Gaussian processes the psd can be specified arbitrarily, whereas for more general random processes the first order pdf constrains the psd.[22] Thus, both for completeness and consistency in a parametric fading channel model, it is desirable to model the channel using Gaussian processes. Furthermore, since a Gaussian process remains Gaussian after linear filtering, any algorithm which generates a sample vector by filtering Gaussian white noise from a random number generator implicitly assumes that the underlying process is Gaussian (possibly modulated later by some type of non-linearity). By making this assumption explicit in the model of the fading channel, any synthetic signal which reproduces the model specification can be assumed to be statistically equivalent regardless of the particular algorithm used to generate the sample vector.

Although the received power signal itself cannot generally be modeled as a Gaussian process, combined with zero-memory non-linearities, Gaussian processes can be used to model the processes underlying both pointing-induced fade and scintillation in weak turbulence,[9,12] as well as the fluctuations in instantaneous coupling efficiency for receivers coupling to few-mode fibers (see Section 4). In the following sections, we develop analyses to reduce sophisticated optical link models to simple parametric models based on Gaussian processes suited for practical engineering purposes.

3. ENGINEERING MODEL FOR SLANT-PATH SCINTILLATION WITH APERTURE-AVERAGING

In the case of weak scintillation, it has been shown that the amplitude of a beam $u(\vec{r}) = e^{\chi+i\phi}$ propagating through atmospheric turbulence obeys log-normal statistics (we are concerned here with modeling space-to-ground downlinks within the weak fluctuation regime and do not consider a parameterization of models for moderate to strong fluctuations). The extension of log-normality to the intensity $I = e^{2\chi}$ averaged over an aperture is also well-documented.[10,23,24] Assuming the aperture-averaged log-intensity $\ln \bar{I}$ is a Gaussian process, the fluctuations of the received power $P(t) = \pi a^2 \bar{I}(t)$ over an aperture of radius a is completely specified by the psd $\Phi_{\ln \bar{I}}(\omega; a)$, since the logarithm can be taken as a zero mean process and the variance is obtained via integration of the psd.

3.1 Temporal power spectrum of aperture-averaged irradiance

For space-to-ground downlinks, the beam can be modeled as a plane wave propagating through a random medium with refractive index fluctuations governed by the spatial power spectrum $\Phi_n(\kappa; s)$ and transverse wind speed $V(s)$ given as functions of the path length s along the propagation axis. For fading channels with weak fluctuations we assume the Kolmogorov spectrum $\Phi_n(\kappa; s) = 0.033 C_n^2(s)\kappa^{-11/3}$ where $C_n^2(s)$ is the refractive index structure constant. We neglect the effects of the turbulence inner and outer scales on account of the fact that the aperture radius a and Fresnel length $\sqrt{L/k}$ (where L is the propagation distance through the turbulence and $k = 2\pi/\lambda$ is the wave number) are generally within the inertial subrange for a space-to-ground downlink in weak turbulence.[14] Using the Rytov approximation an analytical expression for the aperture-averaged temporal psd can be written in the form[25]

$$\Phi_{\ln \bar{I}}(\omega; a) = 32\pi^2 k^2 \int_0^L \frac{ds}{V(s)} \int_0^\infty d\xi\, \Phi_n(\kappa; s) \sin^2\left(\frac{L-s}{2k}[\xi^2 + \omega^2/V^2]\right) \left(\frac{2J_1\left(a\sqrt{\xi^2+\omega^2/V^2}\right)}{a\sqrt{\xi^2+\omega^2/V^2}}\right)^2. \quad (1)$$

From a practical engineering point of view, the issue with this expression is that it depends on full path profiles for the structure constant $C_n^2(s)$ and transverse wind $V(s)$. One solution when this information is unavailable is to choose several standard profiles to use for testing different link scenarios. However, the use of standard profiles leaves the impact on the shape of the psd obscured. Instead, we take an alternative approach by developing a parametric model which directly specifies the psd based on a characteristic cutoff frequency and logarithmic slope which nevertheless captures the gross behavior of (1) including the effects of aperture-averaging.

As a starting point we use the engineering approximation for (1) developed by Yura, where the full profiles $C_n^2(s)$ and $V(s)$ are replaced by an effective turbulent propagation length L_{eff} and rms wind V_{eff} defined by

$$L_{\text{eff}} = \left(\frac{18\int_0^L ds\, C_n^2(s)(L-s)^2}{11\int_0^L ds\, C_n^2(s)(L-s)^{5/6}}\right)^{6/7}, \qquad V_{\text{eff}} = \left(\frac{\int_0^L ds\, C_n^2(s)(L-s)^{5/6} G(L-s,a) V^2(s)}{\int_0^L ds\, C_n^2(s)(L-s)^{5/6} G(L-s,a)}\right)^{1/2}, \quad (2)$$

where $G(s,a)$ is a weighted integral of the Kolmogorov refractive index spectrum approximated by

$$G(s,a) \simeq \frac{1}{1 + 0.754(a^2k/s)^{7/6}}. \quad (3)$$

Using these definitions, it was found that the full path-dependent psd (1) is well-approximated by the psd for constant turbulence conditions

$$\Phi_{\ln \bar{I}}(\omega; a) = \frac{\sigma^2_{\ln \bar{I}}(a)}{\mathcal{N}(\omega_F/\omega_a)} \int_0^\infty d\Omega \, \frac{1 - \mathrm{sinc}\left[(\Omega^2+\omega^2)/\omega_F^2\right]}{\omega_F^2 \left[(\Omega^2+\omega^2)/\omega_F^2\right]^{11/6}} \left(\frac{2J_1\left(\sqrt{(\Omega^2+\omega^2)/\omega_a^2}\right)}{\sqrt{(\Omega^2+\omega^2)/\omega_a^2}} \right)^2 \tag{4}$$

which is completely determined up to the total variance by the effective Fresnel angular frequency $\omega_F = V_{\mathrm{eff}}/\sqrt{L_{\mathrm{eff}}/k}$ and aperture angular frequency $\omega_a = V_{\mathrm{eff}}/a$ (the precise form of the normalization factor $\mathcal{N}(\omega_F/\omega_a)$ is not needed for our purposes). Thus, Yura's approximation reduces the uncountable degrees of freedom required to specify the psd for slant-path channels using the full profiles $C_n^2(s)$ and $V(s)$ to just three parameters ω_F, ω_a and $\sigma^2_{\ln \bar{I}}$. Measurements confirming the general behavior described by (4) can be found in the literature including analyses of the effects of apodized apertures and obscurations.[26]

We now employ this approximation to develop an engineering model eliminating the precise form of the integral (4) in favor of a model that directly parameterizes the general structure of the temporal spectrum. Although the psd exhibits a two-scale structure defined by ω_F and ω_a, as a practical matter we can simplify the model by separating the behavior into three regimes where a single-scale model can be given based on the prevailing behavior. In place of the pair of characteristic frequencies ω_a and ω_F, our single-scale model is based on Yura's scintillation bandwidth

$$\omega_s = \frac{\omega_F}{\sqrt{1 + (\omega_F/\omega_a)^2}} \tag{5}$$

which generally represents the smaller of the two characteristic frequencies. This is the dominant scale in that it determines the correlation time τ_c associated to the exact psd (4)—taken as the lag at which the autocovariance is reduced by 0.315—to an excellent approximation via $\tau_c \simeq 1/\omega_s$.

The behavior of (4) can be separated into three regimes, a small-aperture regime $\omega_F/\omega_a < 1/4$, an intermediate regime $1/4 \leq \omega_F/\omega_a \leq 3$, and a large-aperture regime $\omega_F/\omega_a > 3$ shown in Figure 1. In each case, we

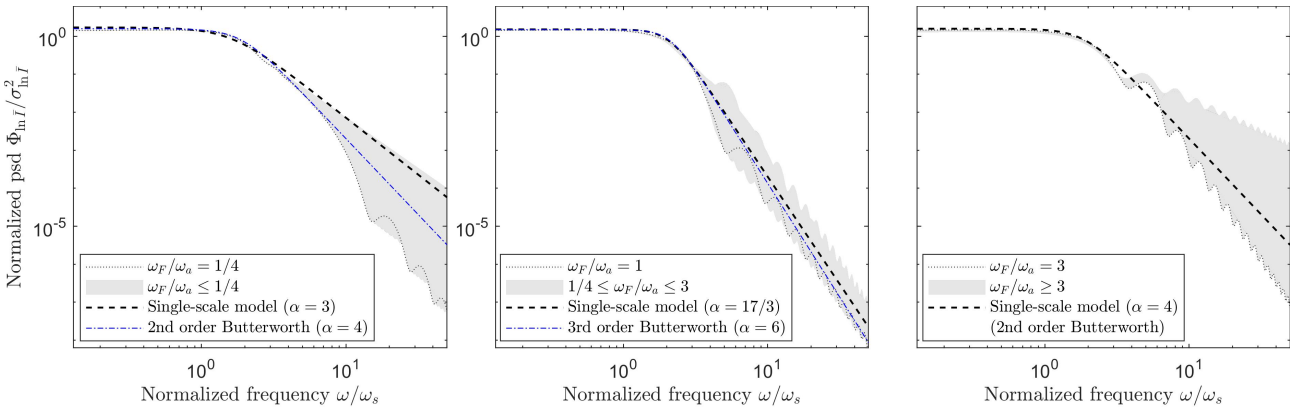

Figure 1. Single-scale model for the temporal power spectrum of aperture-averaged irradiance fluctuations in weak turbulence. The left panel shows upper and lower bounds for the normalized psd for small apertures $\omega_F/\omega_a \leq 1/4$. Similarly, the center and right panels show bounds for intermediate apertures $1/4 \leq \omega_F/\omega_a \leq 3$ and large apertures $\omega_F/\omega_a > 3$, respectively. This single-scale approximation in each regime is determined by the cutoff frequency ω_c and logarithmic slope α discussed in the text.

model the psd (up to normalization) with the same functional form

$$\bar{\Phi}(\omega) = \frac{1}{1 + (\omega/\omega_c)^\alpha} \tag{6}$$

determined by a single cutoff frequency ω_c and logarithmic slope α. The cutoff frequency ω_c is chosen based on the correlation time τ_c. The relation between the 3 dB cutoff ω_c and the correlation time τ_c for the psd (6) is given by $\omega_c \tau_c = K(\alpha)$ where the constant $K(\alpha)$ depends on the slope and is roughly approximated by

$$K(\alpha) \simeq 2.32^{1 - 3.86\alpha^{-2}} \tag{7}$$

for $\alpha \geq 1$. Using this single-scale model for the psd, we first determine the slope α and then set

$$\omega_c = K(\alpha)\omega_s. \tag{8}$$

Many satellite downlinks fall within the intermediate range where the prevailing spectral distribution is well-described by an $\alpha = 17/3$ law (center panel of Figure 1). For small apertures $\omega_F/\omega_a < 1/4$, this slope can substantially underestimate the high frequency content in (4), which is also present in experimental data from free-space links with small-aperture receivers.[27] To accomodate this, the approximation shown in the left panel uses an $\alpha = 3$ power law to include the high-frequency behavior with only minor aperture-averaging of the Kolmogorov spectrum. Finally, in the large aperture regime $\omega_F/\omega_a > 3$ we approximate the psd with $\alpha = 4$ to best fit the low frequency content near $\omega \sim \omega_c$. Although this underestimates higher frequencies in (4), from a practical point of view this error is negligible; to wit, for $\omega_F/\omega_a > 3$ aperture-averaging reduces the total variance by a factor of ∼16 or more at which point the amplitude of these high-frequency fluctuations becomes vanishingly small and channel fading is dominated by transmitter pointing error and fluctuations in receiver coupling efficiency.

To generate synthetic fade vectors in real-time, one can apply a digital low-pass filter (LPF) with squared magnitude response $G^2(\omega) = \bar{\Phi}(\omega)$ to the output of a Gaussian random number generator.[9] Although it is a straightforward matter to generate a finite impulse response filter with squared magnitude response given to very high accuracy by (6) using a long impulse response,[22] note that if α is an even integer, the required gain is achieved by a Butterworth LPF of order $\alpha/2$. Figure 1 shows that using $\alpha = 4$ and $\alpha = 6$ in the small- and intermediate-aperture regimes, respectively, also yields a reasonable approximation which allows the use of readily available digital filter design tools to generate continuous fade vectors. The derivation of the appropriate filter parameters above based on analytical models has the benefit of being generally applicable based on aperture size a and site/orbit-specific models for the structure constant $C_n^2(s)$ and wind profile $V(s)$ including satellite tracking slew rates. An alternative approach for estimating filter parameters based on measurements from a series of experimental optical satellite links is presented by Epple.[10] Ideally, consideration of both approaches is important to developing the best model for a given space-to-ground link scenario.

To summarize, assuming log-normal statistics we characterize the aperture-averaged irradiance fluctuations by specifying the logarithm $\ln \bar{I}$ as a Gaussian process with psd given by (6). This model is determined by 3 parameters, the variance $\sigma^2_{\ln \bar{I}}$, slope α, and cutoff frequency ω_c. In the absence of experimental data for a given link scenario, the approach above derives appropriate values for these parameters based on a model for the turbulence strength $C_n^2(s)$, transverse wind $V(s)$, and aperture radius a. Fade vectors are then generated in real-time by spectrally shaping Gaussian white noise from a pseudo-random number generator using a low-pass filter based on the simple functional form (6).[9,22,28]

4. FLUCTUATIONS OF INSTANTANEOUS COUPLING EFFICIENCY FOR MODE-LIMITED RECEIVERS

For large-aperture receivers, the aperture-averaging factor[14]

$$\frac{\sigma^2_{\ln \bar{I}}(a)}{\sigma^2_{\ln \bar{I}}(0)} \simeq \frac{1}{(1 + 1.07(\omega_F/\omega_a)^2)^{7/6}} \tag{9}$$

can significantly suppress the impact of fluctuations in power over the receiving aperture. However, for larger apertures turbulence can also impact the receiver's ability to efficiently couple light from the receiving aperture to the detector. For passive fiber-coupled systems (without adaptive optics), there is a fundamental limitation to the average efficiency determined by the coupling parameter[18]

$$\eta_0 = \frac{M}{(1 + (D/r_0)^{5/3})^{6/5}} \tag{10}$$

where M is the number of optical modes guided by the fiber (restricting to a single polarization), $D = 2a$ is the aperture diameter, and r_0 is the atmospheric coherence diameter. For mode-limited systems $M < (D/r_0)^2$, the

average coupling efficiency $\langle\eta\rangle$ can be significantly reduced, and is approximated by η_0 when $\eta_0 \ll 1$. In addition to reducing the average efficiency, the instantaneous coupling efficiency $\eta(t)$ can also fluctuate significantly in mode-limited systems and so must be taken into account when modeling the fading channel. Previous theoretical analyses have found that the coupling efficiency to single-mode fiber can be modeled by a Rice distribution in $\sqrt{\eta}$.[15] In this section, we analyze the pdf when coupling to few-mode fibers.

To study these fluctuations for general fiber-coupled systems, we assume a simple focusing system is employed to couple the light from the aperture to the fiber entrance plane modeled via a Fourier transform relation.[18] We numerically simulate the instantaneous coupling efficiency by generating an ensemble of large (4096×4096) Kolmogorov phase screens $u(x,y) = e^{i\phi(x,y)}$ with specified coherence diameter r_0.[20] For each screen, we apply an aperture mask defined by a circular pupil function $\mathcal{P}(x,y)$ and slide the mask over the screen diagonally by one pixel per timestep. The fiber modes are modeled using the scalar LP modes for a step-index fiber. Each set of LP modes is specified by the V-number. The coupling coefficients are calculated by numerically back-propagating the fiber modes to the aperture plane assuming the numerical aperture of the focusing system is equal to the numerical aperture of the fiber, which provides a good estimate of the optimal NA ratio for step-index fibers in general turbulence conditions $\eta_0 < 4$ (including all of the simulations described below).[19] The complex coupling coefficients $c_{lm}(t)$ and efficiency $\eta_{lm}(t) = |c_{lm}(t)|^2$ are calculated for each mode LP_{lm} (including both even and odd parity for $l > 0$), whereupon the instantaneous coupling efficiency is obtained via the sum over all guided modes $\eta(t) = \sum \eta_{lm}(t)$.

4.1 Few-mode fiber coupling efficiency pdf in the low-efficiency regime

To start, we consider the limiting case $\eta_0 \ll 1$ (the limit $\eta_0 \gg 1$ is trivial since the fluctuations vanish in the high-efficiency regime). In the low-efficiency regime $\eta_0 \ll 1$, each mode couples with the same average efficiency

$$\langle\eta_{lm}(t)\rangle \equiv \frac{\langle\eta(t)\rangle}{M} \simeq \frac{\eta_0}{M} = \frac{1}{(1+(D/r_0)^{3/5})^{6/5}}. \tag{11}$$

The equivalence of the average coupling efficiency into each mode in the low-efficiency regime can be derived from the fact that that the atmospheric Wigner distribution for an ensemble of Kolmogorov phase screens with circular pupil is roughly uniform over the phase space domain supporting the guided fiber modes when $\eta_0 \ll 1$.[18,19]

From the numerical simulation using Kolmogorov phase screens and a range of fiber mode sets listed in Table 1, we find that the complex coefficients $c_{lm}(t)$ are described by a circularly-symmetric complex normal distribution, i.e. the real and imaginary parts are independent, normally distributed random variables with equal variance σ_1^2 and zero-mean in the limit $\eta_0 \ll 1$, in agreement with previous theoretical analyses of SMF coupling.[15] As a result, the mode coupling efficiency $\eta_{lm}(t)$ for each individual mode is found to be distributed according to an exponential distribution $\mu_1 e^{-x/\mu_1}$ with mean $\mu_1 = 2\sigma_1^2$ and variance $1/\mu_1^2$. Assuming these complex normal statistics for c_{lm}, we can derive the variance for the mode coupling efficiency η_{lm} for a single mode from our knowledge of the average efficiency $\mu_1 \simeq \eta_0/M$.

If the coupling efficiency for each mode were independent, the total instantaneous coupling efficiency would be gamma distributed $p_\eta(x;k,\theta) = [\theta^{-k}/\Gamma(k)]x^{k-1}e^{-x/\theta}$ with $k = M$ degrees of freedom and scale parameter $\theta = \mu_1 \simeq \eta_0/M$; however, numerical simulations show that correlations exist between the instantaneous coupling efficiency of distinct modes even in the limit $\eta_0 \ll 1$. Nevertheless, the Monte Carlo analysis yields a pdf which can still be modeled by a gamma distribution; albeit with fewer degrees of freedom $k \leq M$. By matching the mean and variance, we obtain the fit shown in Figure 2, with the shape parameter k given in Table 1. As an approximation, the number of degrees of freedom k is roughly given by the number of distinct azimuthal orders $l = 0, 1, ..., k_l - 1$ guided by the fiber, at least up to $k_l = 7$.

Assuming the gamma distribution described above with $k = k_l$ degrees of freedom, the variance of the instantaneous coupling efficiency can be expressed in terms of the mean coupling efficiency $\langle\eta\rangle$ as

$$\sigma_\eta^2 = \frac{\langle\eta\rangle^2}{k_l} \simeq \frac{\eta_0^2}{k_l}. \tag{12}$$

In particular, in the low-efficiency regime $\eta_0 \ll 1$ the normalized variance $\sigma_\eta^2/\langle\eta\rangle^2 \sim 1/k_l$ is independent of the severity of turbulence. The $\sqrt{k_l}$ proportionality between the mean $\langle\eta\rangle$ and deviation σ_η for $\eta_0 \ll 1$ is shown in Figure 3. This relation is seen to hold for $\eta_0 \simeq \langle\eta\rangle < 0.25$, at which point the variance starts to level off.

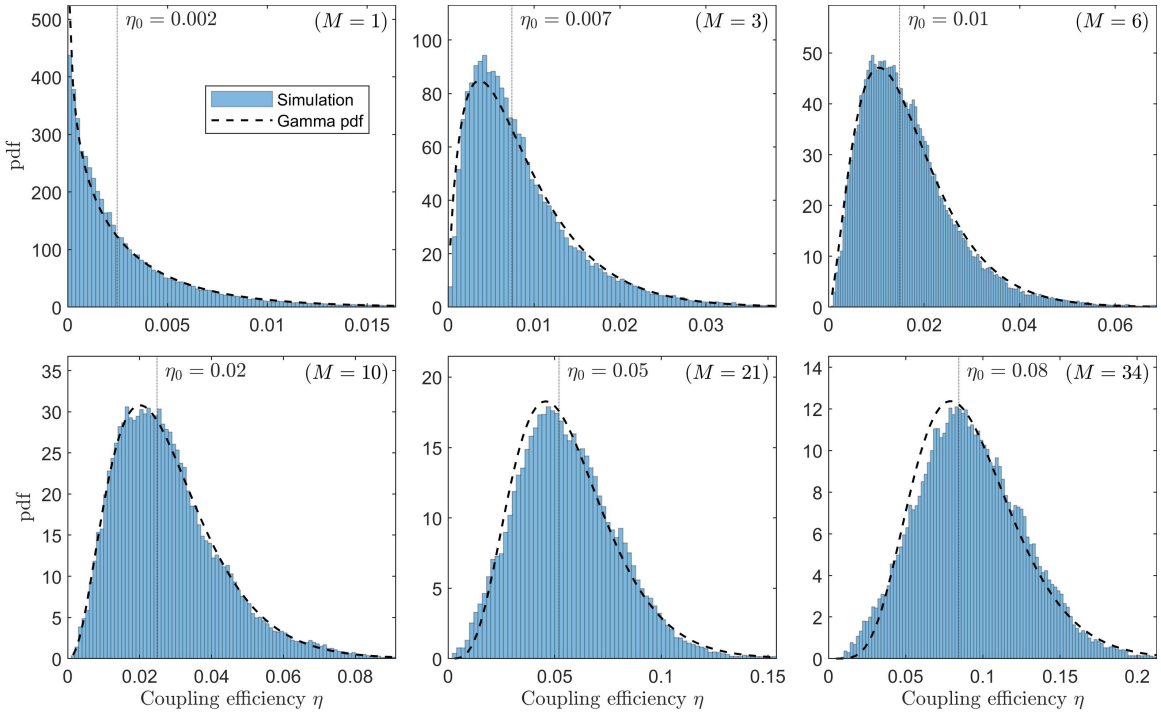

Figure 2. Probability density function for the passive coupling efficiency into step-index fibers with M scalar modes from Monte Carlo simulation with Kolmogorov phase screens in the low-efficiency regime $\eta_0 < 0.1$. The fit for the gamma distribution is determined using the mean and variance.

Coupling parameter η_0	$\eta_0 < 0.1$																	$\eta_0 \geq 0.1$	
# Guided scalar modes M	1	3	6	8	10	12	15	17	19	21	23	25	27	30	34	36	38	40	42
V-number	2.3	3.7	5	5.4	6.3	6.9	7.4	8.3	8.5	8.7	9.6	9.8	10.1	10.9	11.5	11.7	12.1	12.3	12.9
Az. orders $k_l = l_{\max} + 1$	1	2	3	4	4	5	5	6	6	6	7	7	8	8	8	9	9	10	10
Shape parameter k	0.8	2.0	2.9	3.3	3.6	4.8	4.6	5.5	5.8	5.7	6.4	6.7	6.6	6.3	7.4	8.0	8.0	7.2	8.2

Table 1. Shape parameter k for Gamma distribution fit for coupling efficiency pdf in low-efficiency regime $\eta_0 \ll 1$. Fit based on mean and variance calculated from Monte Carlo simulation using Kolmogorov phase screens with $D/r_0 = 20$.

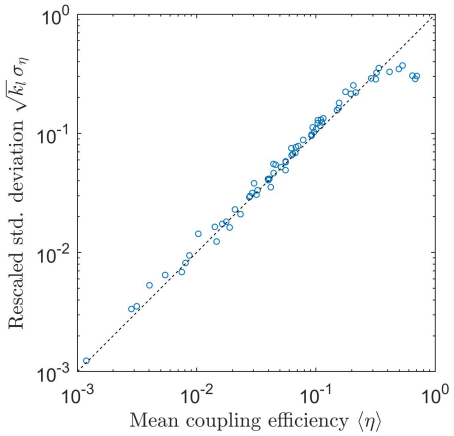

Figure 3. Standard deviation σ_η of coupling efficiency for step-index fibers with $1 \leq M \leq 42$ and $5 \leq D/r_0 \leq 30$. The vertical axis is obtained by normalizing by $1/\sqrt{k_l}$, where k_l is the number of distinct azimuthal orders guided by the fiber.

4.2 Few-mode fiber coupling efficiency pdf in the moderate and high-efficiency regime

In the moderate and high-efficiency regimes $\eta_0 > 0.1$, the gamma distribution no longer yields a good model for turbulence-induced coupling fluctuations for an arbitrary number of guided modes M. As mentioned above, in the SMF case it has been found that the pdf can be modeled by a Rice distribution;[15] however, there are two effects that complicate the statistics for few-mode fibers. First, for $\eta_0 > 0.1$ the turbulence-distorted light now concentrates preferentially in low order modes (a result of the non-uniformity of the atmospheric Wigner distribution over the phase space acceptance of the fiber).[19] Second, the onset of saturation of the total efficiency forces additional correlations between the amount of light coupled into distinct modes. In the absence of an analytical model, Monte Carlo simulations can be used in this regime to obtain a numerical approximation of the pdf. Examples of pdfs obtained in the saturation regime are shown in Figure 4.

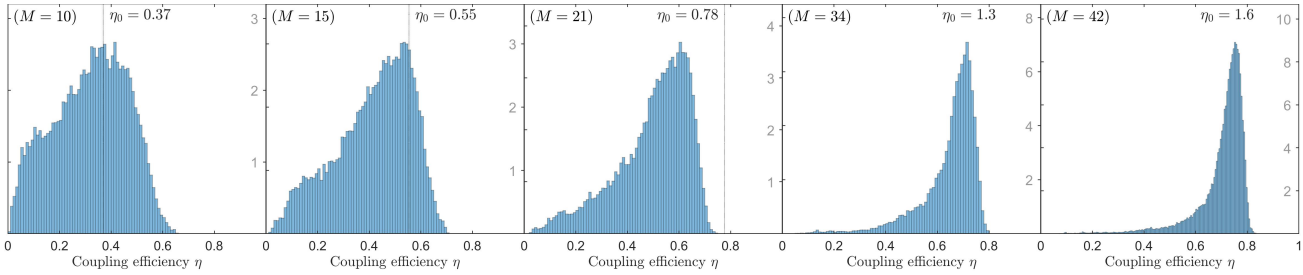

Figure 4. Probability density function of passive coupling efficiency into step-index fibers with M guided modes in the saturation regime $\eta_0 > 0.3$. Calculated from Monte Carlo simulation using Kolmogorov phase screens with $D/r_0 = 5$.

4.3 Temporal power spectrum of instantaneous coupling efficiency

The power spectral density of the instantaneous coupling efficiency was calculated based on the Monte Carlo simulations described above for fibers with $1 \leq M \leq 42$ using Kolmogorov phase screens with $D/r_0 = 5, 10$, and 20. As a first approximation, we find that the temporal power spectrum is largely independent of the coupling parameter η_0 and number of guided modes M, aside from an overall scaling by the total variance of the fluctuations. Normalizing by the total variance, the maximum and minimum range of the psd is shown by the shaded region in Figure 5, along with a typical example obtained for coupling into a 21-mode fiber with $D/r_0 = 10$.

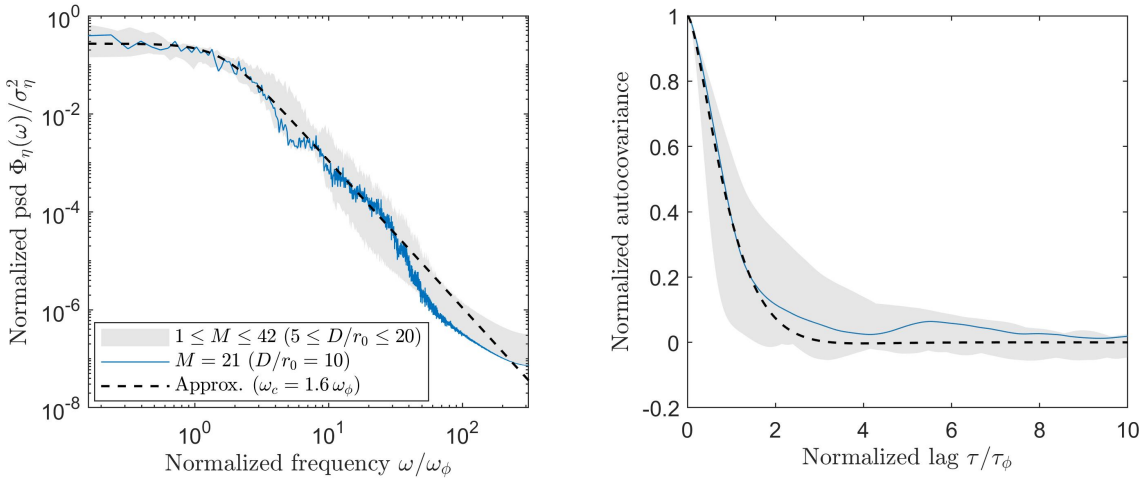

Figure 5. Temporal power spectral density and autocovariance for the instantaneous coupling efficiency for a range of few-mode fibers. The shaded region gives the upper and lower bounds for all simulated fibers with $1 \leq M \leq 42$ using Kolmogorov phase screens with $D/r_0 = 5, 10$, and 20. The blue curve gives a typical example from the middle of this range with $M = 21$ and $D/r_0 = 10$. The lag is normalized by the characteristic time $\tau_\phi = 1/\omega_\phi$.

In a coarse approximation, we find that the general behavior is characterized by the characteristic aperture angular frequency $\omega_\phi = V_\phi/a$ where V_ϕ is the velocity of the phase screen and $a = D/2$ is the radius of the aperture. Noting that the psd is roughly flat up to an aperture cutoff ω_c, we can again model the generic behavior using the simple functional form (6)

$$\Phi_\eta(\omega;\omega_c) = \sigma_\eta^2 \frac{\sqrt{27}}{2\omega_c} \cdot \frac{1}{1+(\omega/\omega_c)^3} \tag{13}$$

exhibiting a power law decay with exponent $\alpha = 3$ (this is an empirical fit which combines a natural -8/3 power law with a subtle low-pass filtering effect discussed in the next section). Within this range of fibers and turbulence conditions, the cutoff frequency remained within the range

$$\omega_\phi \leq \omega_c \leq 3\omega_\phi. \tag{14}$$

Correspondingly, the temporal correlation time increased with the number of modes but only within a factor of 3 within this range of fibers and turbulence conditions (the maximum and minimum of the normalized temporal autocovariance is also shown in Figure 5). Although this coarse approximation ignores some subtle effects of the mode structure of the fiber discussed below, it suffices to capture the generic behavior. As such it yields a simple a parametric model where the cutoff frequency can be chosen within the bounds (14) based on estimates for the phase velocity V_ϕ.

It is important to note that for inclined propagation paths with non-uniform turbulence, the phase screen velocity V_ϕ is generally very different than the effective rms wind V_{eff} relevant for the aperture-averaged irradiance fluctuations. For space-to-ground links, the velocity V_ϕ relevant for fluctuations in coupling efficiency is dominated by strong turbulence close to the ground receiver, whereas the effective rms wind V_{eff} is weighted towards the velocity of the turbulent medium farther from the receiver where the additional propagation distance allows space for irradiance fluctuations to develop. As wind speeds and transverse air speeds from satellite tracking generally increase farther from the ground receiver, one can expect much longer correlation times for fluctuations from fiber coupling (i.e. on the order of the inverse Greenwood frequency) compared to the shorter correlation times associated to irradiance flucuations.

4.3.1 The effect of few-mode fiber mode structure on the temporal power spectrum

To illustrate the effect of the few-mode fiber on the temporal spectrum, Figure 6 shows the power spectral density for 3 fibers with $M = 1, 6$ and 21 guided modes using a phase screen with $D/r_0 = 10$.

Similar to the manner in which aperture-averaging acts as a low pass filter on irradiance fluctuations in the aperture, the fiber modes can be seen to act as a low pass filter for the phase fluctuations in the aperture. Specifically, we note that the single-mode fiber does not admit the higher frequency fluctuations admitted by the 6-mode and 21-mode fibers. This low-pass effect is also in evidence in the panel on the right, which shows the power spectrum for the coupling efficiency η_{lm} of each individual mode in the 6-mode fiber. Observe that the roll-off frequency for the individual modes increases with the mode order, with the exception of the LP_{02} and LP_{21} modes which have the same roll-off frequency. This can be attributed to the fact that these two modes have the same V-number cutoff of 3.832.

It is worth noting that the fiber low-pass effect is fundamentally different than the aperture-averaging low-pass effect. Although the temporal correlation time increases with size of the fiber core just as it does with the size of the aperture, the fiber low-pass effect acts in the opposite manner in the sense that the larger core fibers with more modes also admit more high-frequency noise. Conversely, the larger apertures have the opposite effect of suppressing the high-frequency noise from irradiance fluctuations at the aperture plane.

More precisely, as the fiber accepts higher order modes, the temporal power spectrum can be seen to develop the -8/3 law behavior expected from the unfiltered Kolmogorov phase spectrum (left panel of Figure 6). For fibers which only carry a small number of modes, the domain supporting the -8/3 law power spectrum shrinks as higher frequency phase fluctuations in the aperture are filtered out. The cutoff frequency at which the 8/3 law yields to a hard roll-off depends on the highest order mode carried by the fiber.

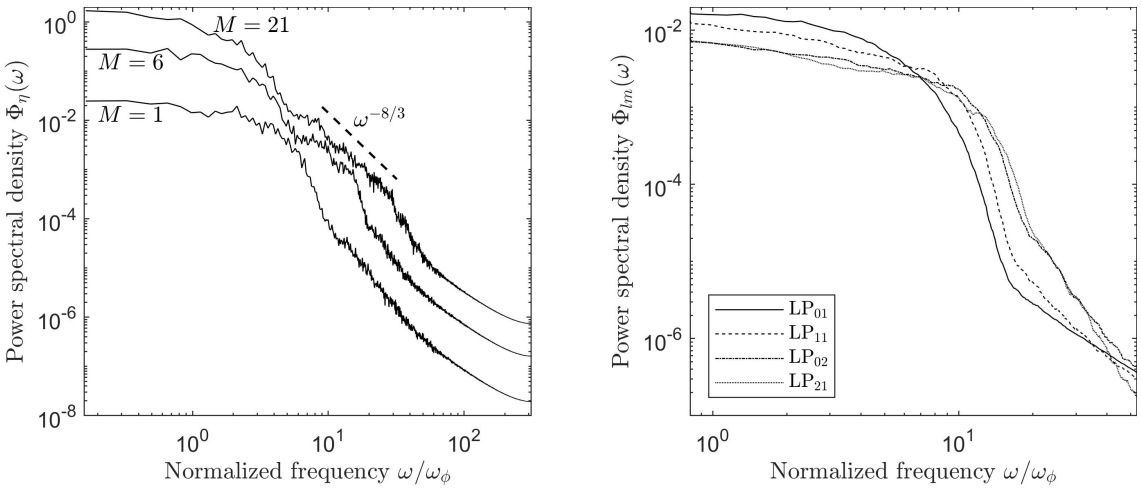

Figure 6. The left panel shows the power spectral density of coupling efficiency $\Phi_\eta(\omega)$ for step-index fibers with $M = 1, 6$ and 21 guided modes (from bottom to top). The right panel decomposes the temporal spectrum of the 6-mode fiber, showing the temporal spectrum of the individual mode coupling efficiency η_{lm}. Both results are calculated from Monte Carlo simulation using Kolmogorov phase screens with $D/r_0 = 10$.

4.4 Real-time generation of synthetic fade vectors for instantaneous coupling efficiency

Finally, we summarize the results above and propose an algorithm for real-time generation of fade vectors representing fluctuations in the instantaneous coupling efficiency for receivers coupling to few-mode fibers. The following is based on the assumption that the log-amplitude and phase of the optical field are uncorrelated, so that the total fade vector can be constructed by combining the aperture-averaged irradiance fluctations and coupling efficiency fluctuations as independent processes.

In the low-efficiency regime $\eta_0 < 0.1$ the pdf can be modeled by a gamma distribution $p_\eta(x; k_l, \eta_0/k_l)$ with mean η_0, variance $\sigma_\eta^2 \simeq \eta_0^2/k_l$, and k_l degrees of freedom. Since k_l is a positive integer this distribution can be obtained from a sum of k_l independent random variables $C_i(t)$ each obeying an exponential distribution with mean η_0/k_l. The variables $C_i(t)$ can in turn be synthesized by generating $2k_l$ parallel Gaussian processes, as follows.

For each process $C_i(t)$, a pair of normally distributed random variables $a_i(t)$ and $b_i(t)$ is produced by a Gaussian random number generator with zero mean and variance $\sigma_i^2 = \eta_0/2k_l$. Each of these random vectors are passed through a low-pass filter to produce the desired psd (13) (specified by a cutoff frequency $\omega_c \simeq \omega_\phi$ and slope $\alpha = 3$). The independent exponential variables $C_i(t) = a_i(t)^2 + b_i(t)^2$ are then produced from the sum of squares of the Gaussian random variables a_i and b_i. The instantaneous coupling efficiency is then constructed as the sum

$$\eta(t) = \sum_{i=1}^{k_l} C_i(t). \tag{15}$$

Assuming the psd is preserved by the sum of squares—a generally acceptable assumption for a simple zero-memory non-linearity[28]—the result is a gamma distributed random process $p_\eta(x; k_l, \eta_0/k_l)$ with mean η_0, variance η_0^2/k_ℓ, exhibiting the desired temporal power spectrum (13).

Unfortunately, this technique does not apply in the moderate and high-efficiency regime $\eta_0 > 0.1$ due to the complex structure of the pdf (Figure 4), and also does not take into account any effects from tilt-compensation on the pdf. In the absence of an analytical model of the pdf, one must resort to Monte Carlo simulations. For example, such simulations can be used to numerically approximate the pdf, whereupon standard methods can be used to generate a fading signal with the resulting pdf and psd (13) from a Gaussian random number generator.[22,28] Alternatively, if one can continuously generate long Kolmogorov phase screens in real-time, fade vectors can be produced directly by using the simulation technique employed in this work.

5. CONCLUSIONS

An analysis of turbulence-induced fade over atmospheric channels was presented focused on producing practical engineering models suitable for synthesizing fading power vectors in real-time. Using Yura's approximation, a simple model for aperture-averaged scintillation as a Gaussian process parameterized by the variance, cutoff frequency, and slope was developed for general slant-path channels (Section 3). Finally, a Monte Carlo analysis of fluctuations in the instantaneous coupling efficiency for receivers coupling to few-mode fibers was presented. This analysis enables a simplified receiver test setup by including fluctuations in coupling efficiency directly in the model of the fading channel used to generate fade vectors without requiring real-time emulation of the turbulence-distorted optical wavefront arriving at the telescope. The temporal power spectrum of these fluctuations was generally characterized by a single cutoff frequency (14) and logarithmic slope $\alpha = 3$. A parametric model for the pdf was obtained in the low-efficiency regime $\eta_0 < 0.1$ based on a gamma distribution, parameterized by the mean efficiency η_0 and number of distinct azimuthal mode orders k_l guided by the fiber. A explicit algorithm was proposed for real-time generation of fade vectors modeling the instantaneous coupling efficiency in the low-efficiency regime. Methods for modeling the more complex pdf obtained in the moderate to high-efficiency regime were discussed, though a parametric model was not obtained for this case. Such a model requires a better understanding of the fluctuations in the coupling efficiency in this regime and is left for future consideration. The results presented in this manuscript are based on analytical models and simulation. Direct comparison of these models to experimental fade measurements, particularly with regard to the ITU recommendations for quantifying Earth-space fade dynamics,[29] is still needed.

ACKNOWLEDGMENTS

This work is supported by the NASA Space Communications and Navigation (SCaN) Program and the Glenn Research Center Communications & Intelligent Systems Division.

REFERENCES

[1] Toselli, I., Andrews, L. C., Phillips, R. L., and Ferrero, V., "Free space optical system performance for a gaussian beam propagating through non-kolmogorov weak turbulence," *IEEE Transactions on Antennas and Propagation* **57**(6), 1783–1788 (2009).

[2] Rabinovich, W. S., Mahon, R., Ferraro, M. S., Moore, C. I., and Coffee, A., "Optical propagation in a marine environment: effects of turbulence spectrum choice on simulation," in [*Free-Space Laser Communications XXXIV*], Hemmati, H. and Robinson, B. S., eds., **11993**, 119930J, International Society for Optics and Photonics, SPIE (2022).

[3] Andrews, L. C., Phillips, R. L., Wayne, D., Leclerc, T., Sauer, P., Crabbs, R., and Kiriazes, J., "Near-ground vertical profile of refractive-index fluctuations," in [*Atmospheric Propagation VI*], Thomas, L. M. W. and Gilbreath, G. C., eds., **7324**, 11 – 22, International Society for Optics and Photonics, SPIE (2009).

[4] Andrews, L. C., Phillips, R. L., and Hopen, C. Y., "Aperture averaging of optical scintillations: power fluctuations and the temporal spectrum," *Waves in Random Media* **10**(1), 53–70 (2000).

[5] Andrews, L. C., Phillips, R. L., and Young, C. Y., "Scintillation model for a satellite communication link at large zenith angles," *Optical Engineering* **39**(12), 3272 – 3280 (2000).

[6] Rabinovich, W. S., Mahon, R., Ferraro, M. S., Murphy, J. L., and Moore, C. I., "Scintillation recording and playback in free-space optical links," *Optical Engineering* **55**(11), 111613 (2016).

[7] Roth, J. M., Rauch, S., Reynolds, B., Schieler, C. M., and Ulmer, T. G., "Forward error correction and interleaving performance for lasercom terminals in fading channels," in [*Free-Space Laser Communications XXXIV*], Hemmati, H. and Robinson, B. S., eds., **11993**, 1199307, International Society for Optics and Photonics, SPIE (2022).

[8] Katz, E. J., Chahine, Y. K., Vyhnalek, B. E., and Tedder, S. A., "Acousto-optic modulator for emulating atmospheric fade in free-space optical communication systems," in [*Free-Space Laser Communications XXXII*], Hemmati, H. and Boroson, D. M., eds., **11272**, 1127219, International Society for Optics and Photonics, SPIE (2020).

[9] Giggenbach, D., Parthasarathy, S., Shrestha, A., Moll, F., and Mata-Calvo, R., "Power vector generation tool for free-space optical links — pvget," in [*2017 IEEE International Conference on Space Optical Systems and Applications (ICSOS)*], 160–165 (2017).

[10] Epple, B., "Simplified channel model for simulation of free-space optical communications," *J. Opt. Commun. Netw.* **2**, 293–304 (May 2010).

[11] Perlot, N., Knapek, M., Giggenbach, D., Horwath, J., Brechtelsbauer, M., Takayama, Y., and Jono, T., "Results of the optical downlink experiment KIODO from OICETS satellite to optical ground station Oberpfaffenhofen (OGS-OP)," in [*Free-Space Laser Communication Technologies XIX and Atmospheric Propagation of Electromagnetic Waves*], Mecherle, S. and Korotkova, O., eds., **6457**, 645704, International Society for Optics and Photonics, SPIE (2007).

[12] Barron, R. J. and Boroson, D. M., "Analysis of capacity and probability of outage for free-space optical channels with fading due to pointing and tracking error," in [*Free-Space Laser Communication Technologies XVIII*], Mecherle, G. S., ed., **6105**, 61050B, International Society for Optics and Photonics, SPIE (2006).

[13] Fried, D. L., "Statistics of laser beam fade induced by pointing jitter," *Appl. Opt.* **12**, 422–423 (Feb 1973).

[14] Yura, H. T., "Optical downlink propagation from space-to-earth: aperture-averaged power fluctuations, temporal covariance and power spectrum," *Opt. Express* **26**, 26787–26809 (Oct 2018).

[15] Ma, J., Ma, L., Yang, Q., and Ran, Q., "Statistical model of the efficiency for spatial light coupling into a single-mode fiber in the presence of atmospheric turbulence," *Appl. Opt.* **54**, 9287–9293 (Nov 2015).

[16] Ma, L., Gao, S., Chen, B., and Liu, Y., "Theoretical and experimental analysis on statistical properties of coupling efficiency for single-mode fiber in free-space optical communication link based on non-kolmogorov turbulence," *Applied Sciences* **12**(12) (2022).

[17] Yang, Q., Li, L., Guo, P., Wang, Q., Yu, S., Tan, L., and Ma, J., "Ground equivalent verification for atmospheric turbulence effects on fiber-coupling efficiency of satellite-to-ground downlink," *Optical Engineering* **57**(12), 126102 (2018).

[18] Chahine, Y. K., Tedder, S. A., Staffa, J., and Vyhnalek, B. E., "Optimal efficiency for passively coupling partially coherent light into mode-limited optical waveguides," *J. Opt. Soc. Am. A* **38**, 1732–1743 (Dec 2021).

[19] Chahine, Y. K., Rushton, F., Vyhnalek, B. E., and Tedder, S. A., "Numerical phase space optics methods and applications to the analysis of fiber coupling efficiency in atmospheric turbulence," in [*Free-Space Laser Communications XXXIV*], Hemmati, H. and Robinson, B. S., eds., **11993**, 119930U, International Society for Optics and Photonics, SPIE (2022).

[20] Simon Ellis, Jonathan Bland-Hawthorn, S. L.-S., "General coupling efficiency for fibre fed astronomical instruments," *J. Opt. Soc. Am. B* (2021).

[21] Goodman, J. W., [*Statistical optics*] (1985).

[22] Sondhi, M. M., "Random processes with specified spectral density and first-order probability density," *The Bell System Technical Journal* **62**(3), 679–701 (1983).

[23] Fried, D. L., "Aperture averaging of scintillation," *J. Opt. Soc. Am.* **57**, 169–175 (Feb 1967).

[24] Mitchell, R. L., "Permanence of the log-normal distribution∗," *J. Opt. Soc. Am.* **58**, 1267–1272 (Sep 1968).

[25] Wheelon, A., [*Electromagnetic Scintillation: Volume 2, Weak Scattering*], Cambridge University Press (2003).

[26] Dravins, D., Lindegren, L., Mezey, E., and Young, A. T., "Atmospheric Intensity Scintillation of Stars. III. Effects for Different Telescope Apertures," *Publications of the Astronomical Society of the Pacific* **110**, 610–633 (May 1998).

[27] Chahine, Y. K., Wroblewski, A. C., Malowicki, J. E., Flatico, J. M., Ristroph, G., Hsia, A., Megally, R., and Resnick, A., "Laser beam propagation simulations of long-path scintillation and fade with comparison to ground-to-aircraft optical link measurements," *Optical Engineering* **60**, 036112 (Mar. 2021).

[28] Gujar, U. and Kavanagh, R., "Generation of random signals with specified probability density functions and power density spectra," *IEEE Transactions on Automatic Control* **13**(6), 716–719 (1968).

[29] "Prediction method of fade dynamics on Earth-space paths," *International Telecommunication Union (ITU), Recommendation ITU-R P.1623-1* (2005).